

## Near-field radiative heat transfer between doped-Si parallel plates separated by a spacing down to 200 nm

Jesse I. Watjen, Bo Zhao, and Zhuomin M. Zhang

Citation: [Applied Physics Letters](#) **109**, 203112 (2016); doi: 10.1063/1.4967384

View online: <http://dx.doi.org/10.1063/1.4967384>

View Table of Contents: <http://scitation.aip.org/content/aip/journal/apl/109/20?ver=pdfcov>

Published by the [AIP Publishing](#)

---

### Articles you may be interested in

[Electrically tunable near-field radiative heat transfer via ferroelectric materials](#)

Appl. Phys. Lett. **105**, 244102 (2014); 10.1063/1.4904456

[Graphene-assisted near-field radiative heat transfer between corrugated polar materials](#)

Appl. Phys. Lett. **104**, 251911 (2014); 10.1063/1.4885396

[Near-field radiative heat transfer between doped silicon nanowire arrays](#)

Appl. Phys. Lett. **102**, 053101 (2013); 10.1063/1.4790143

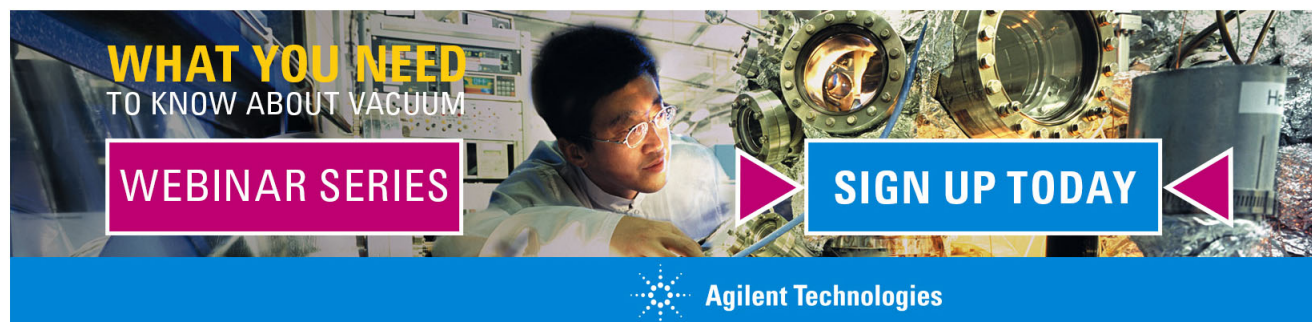
[Near-field radiative transfer based thermal rectification using doped silicon](#)

Appl. Phys. Lett. **98**, 113106 (2011); 10.1063/1.3567026

[Radiative heat transfer at nanoscale mediated by surface plasmons for highly doped silicon](#)

Appl. Phys. Lett. **95**, 231913 (2009); 10.1063/1.3271681


---

The advertisement features a background image of a person in a lab coat working with a piece of scientific equipment. Overlaid on this image are several text elements: 'WHAT YOU NEED TO KNOW ABOUT VACUUM' in yellow and white, 'WEBINAR SERIES' in white on a purple rectangular background, and 'SIGN UP TODAY' in white on a blue rectangular background. Two purple arrowheads point towards the 'SIGN UP TODAY' button. At the bottom, the Agilent Technologies logo and name are displayed on a blue background.

**WHAT YOU NEED  
TO KNOW ABOUT VACUUM**

**WEBINAR SERIES**

**SIGN UP TODAY**

 **Agilent Technologies**

# Near-field radiative heat transfer between doped-Si parallel plates separated by a spacing down to 200 nm

Jesse I. Watjen,<sup>a)</sup> Bo Zhao,<sup>a)</sup> and Zhuomin M. Zhang<sup>b)</sup>

George W. Woodruff School of Mechanical Engineering, Georgia Institute of Technology, Atlanta, Georgia 30332, USA

(Received 4 July 2016; accepted 27 October 2016; published online 15 November 2016)

Heat transfer between two objects separated by a nanoscale vacuum gap holds great promise especially in energy harvesting applications such as near-field thermophotovoltaic systems. However, experimental validation of nanoscale radiative heat transfer has been largely limited to tip-plate configurations due to challenges of maintaining small gap spacing over a relatively large area. Here, we report measurements of heat transfer near room temperature between two 1 cm by 1 cm doped-Si parallel plates, separated by a vacuum gap from about 200 nm to 780 nm. The measured strong near-field radiative transfer is in quantitative agreement with the theoretical prediction based on fluctuational electrodynamics. The largest measured radiative heat flux is 11 times as high as the blackbody limit for the same hot and cold surface temperatures. Our experiments have produced the highest radiative heat transfer rate observed to date across submicron distances between objects near room temperature. *Published by AIP Publishing.*

[<http://dx.doi.org/10.1063/1.4967384>]

The increasing demand for sustainable energy leads to an urgent need for alternative energy harvesting methods with better performance than current technologies. Near-field radiative heat transfer is one of the most promising routes for boosting the efficiency and power output of energy harvesting systems such as thermophotovoltaics.<sup>1</sup> It has been shown that when two objects at different temperatures are brought within a distance much smaller than the characteristic wavelength of thermal radiation, the radiative heat flux can exceed the well-known blackbody limit governed by the Stefan-Boltzmann law by orders of magnitude.<sup>2–4</sup> This effect is caused by the coupling of forward and backward evanescent waves that opens the paths for photons to tunnel from the hot side to the cold side. Theoretically, near-field radiative heat flux scales up with  $d^{-2}$ , where  $d$  is the gap spacing between two parallel plates.<sup>2,5</sup> For energy harvesting applications, increasing the surface area and shrinking the gap spacing are both critical in order to achieve high radiative heating rates. While tremendous progress has been made in recent years toward experimental realization, measurements between planar surfaces with square-centimeter-sized areas at deep submicron gap distances are still quite challenging due to difficulties in controlling the gap spacing.<sup>6</sup> In this work, we experimentally measured the radiative heat transfer between two 1-cm<sup>2</sup> doped-Si plates separated by a vacuum gap spacing from  $(782 \pm 40)$  nm down to  $(200 \pm 80)$  nm. With careful control, thermal radiation dominates the heat transfer and the design may be extended to even larger heat transfer areas with other materials and thus may be implemented in applications such as near-field thermophotovoltaics,<sup>1,7</sup> thermal rectification,<sup>8,9</sup> thermal transistors,<sup>10</sup> and radiative refrigeration.<sup>11,12</sup>

Using complicated experiments enabled by scanning probe microscopy (SPM), researchers have measured the near-field radiative heat transfer between an SPM tip (or a small sphere) and a flat surface at gap distances down to tens of or even a few nanometers.<sup>3,4,13–17</sup> However, this type of configuration has a relatively small area where photon tunneling may occur and thus the heating rate is extremely limited, preventing it for use in applications that require a large photon flux. Continuous efforts have been made to overcome this limitation by measuring near-field thermal radiation between planar (or flat) surfaces, and significant progress has been made in recent years.<sup>18–26</sup> For example, Ito *et al.*<sup>24</sup> measured the near-field heat flux between two fused quartz substrates, with an area of 1.6 cm<sup>2</sup>, at gap spacings down to 500 nm. In the study by St-Gelais *et al.*,<sup>25</sup> a gap spacing near 40 nm was reached but the surface area was much smaller. Very recently, Song *et al.*<sup>26</sup> developed a microdevice that can achieve a spacing down to about 100 nm with surface areas about 50  $\mu$ m by 50  $\mu$ m. However, most of the reported experiments are still limited by either small heat transfer areas or relatively large gap spacings. These limitations can be understood if we consider that, for a perfectly flat 1-cm-wide piece to achieve 100 nm gap spacing, the angle of the piece cannot be off by more than  $6 \times 10^{-4}$  deg. Otherwise, contact between the two plates would occur at the end, and consequently, conduction would dominate the heat transfer. If the non-flatness of the sample surface is also considered, it is almost impossible to maintain a perfect nanometric gap over large areas. Therefore, there naturally exists a tradeoff between the surface area and the parallelism of the gap in practice. In order to benefit the real-world applications using near-field thermal radiation, it is imperative to explore a practical design that can reveal the near-field effect by keeping stringent parallelism between two planar surfaces with a relatively large heat transfer area and that can potentially be scaled up without too much complexity.

<sup>a)</sup>J. I. Watjen and B. Zhao contributed equally to this work.

<sup>b)</sup>Author to whom correspondence should be addressed. Electronic mail: zhuomin.zhang@me.gatech.edu

An experimental platform was developed in the present work for measuring the near-field heat transfer, as shown in Fig. 1(a). The spring presses the stack of layers onto a copper base to form a nearly one-dimensional heat flow path. The lateral dimensions of these layers, as well as the raised base plate, are 1 cm by 1 cm. On top of the stack lays a printed resistance heater (in red color online). A DC power supply provides 10–300 mW to the resistance heater. The heater is epoxied to a 1-mm-thick copper plate (in orange) that is gold plated to reduce the radiative heat loss. The sample (in blue) is sandwiched between two identical copper plates using a thin layer of silver grease to ensure good thermal contact. A tiny hole drilled halfway through the side allows a thermocouple to be inserted on each copper plate to measure the hot-side and cold-side temperatures of the sample,  $T_1$  and  $T_2$ , respectively. The applied power generates a temperature difference ( $\Delta T_1 = T_1 - T_2$ ) about 2–30 K between the copper plates. A thermopile-type heat flux meter (HFM) is epoxied underneath the lower copper plate and atop the raised base plate. A calibrated silicon diode thermistor mounted on the base plate measures the absolute temperature of the heat sink ( $T_0$ ) with an uncertainty of 37 mK. The base plate is screw-fastened to the inside of a vacuum chamber. A thermocouple constructed using nickel-chromium (blue) and constantan (red) wires measures the temperature difference,  $\Delta T_2 = T_2 - T_0$ , in order to determine the cold plate temperature  $T_2$ , while the other measures the temperature difference between the copper plates  $\Delta T_1$  to obtain the absolute temperature  $T_1$ . Aluminum foil (not shown) surrounded the sample stage serves as a radiation shield to reduce the side heat loss. Together with the heat flux measured, the thermal conductance of the sample can be quantified and compared with theoretical predictions. A spring on top of the stack applies a quantifiable force on the sample.

The samples were constructed with two square pieces of doped-Si fabricated from double-side-polished wafers. The upper piece closer to the heater is called the radiation emitter while the lower piece is called the receiver throughout this paper. To create a desired gap spacing between the pieces, a two-dimensional array of  $\text{SiO}_2$  posts was fabricated on one piece using ultraviolet photolithography, as shown in Fig. 1(b).

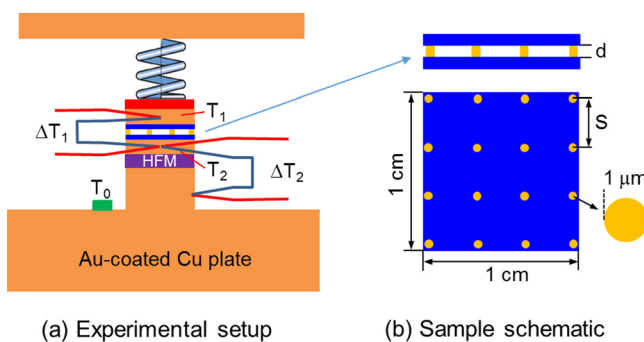


FIG. 1. Schematics of the experimental setup for measuring the near-field radiative heat transfer between flat plates and the structure of the sample. (a) The measurement stage that contains a stack of layers below the spring, namely, a heater, the upper Cu plate, the sample made of two doped-Si plates separated by a gap, the lower Cu plate, and a heat flux meter (HFM) mounted on a Cu heat sink. (b) The sample made of two doped-Si pieces separated by a sub-micron gap using  $\text{SiO}_2$  posts, where  $S$  is the distance between adjacent posts.

$\text{SiO}_2$  was chosen because of its low thermal conductivity, high mechanical strength, and ease of fabrication. The height of the posts varies between samples and ranges from 200 nm to 800 nm. An unpatterned piece was then mated together with the patterned piece in a cleanroom environment to form a sub-micron gap. The gap spacing is controlled by the height of posts and the applied force. Extremely flat wafers with a thickness approximately  $500 \mu\text{m}$  were employed, and a silicon dioxide layer was deposited on the back side of some wafers for bow reduction. The detailed fabrication process is described in the [supplementary material](#). Since the typical size of dust particles is on the order of micrometers, the small gap spacing naturally prevents particulate matter from entering the gap. While the posts maintain mechanical stability of the gap, they also introduce additional pathways for heat to conduct from the emitter to the receiver.

To measure the radiative heat transfer, it is preferred to ensure that thermal radiation is the dominant transfer mode across the sample. Note that the effect of gas conduction is eliminated by maintaining the pressure in the chamber below  $3 \times 10^{-4}$  Pa. Although near-field radiative transfer increases considerably as gap spacings approach the nanometer range, it is still orders of magnitude weaker compared to conduction heat transfer with the same cross-sectional area. Therefore, the number of the posts should be reduced as much as possible while maintaining the gap spacing mechanically. A photomask was made that contains four patterns with different spans between posts, i.e.,  $S$  equals to  $200 \mu\text{m}$ ,  $300 \mu\text{m}$ ,  $400 \mu\text{m}$ , and  $500 \mu\text{m}$ . With a post diameter of approximately  $1 \mu\text{m}$ , it is estimated that more than half of the conductance is due to radiation when  $S$  exceeds about  $300 \mu\text{m}$  (see [supplementary material](#) for details).

Even though the thermal grease was applied, contact resistance could not be completely removed. Thus, after measuring the samples under vacuum, the chamber was returned to ambient pressure where gas conduction across the gap dominates and the thermal resistance of the sample is negligible due to the large thermal conductivity of silicon. Thermal resistances of the Cu plates are also negligible. Thus, the contact resistance at the copper-silicon interfaces can be obtained based on the measured  $T_1$  and  $T_2$  when the chamber is at ambient pressure. It is assumed that the contact resistance is the same above and below the sample. The contact resistance value, ranging from 4 to 9 K/W across each Si-Cu interface, was used to deduce the temperatures of the two Si pieces, i.e., the emitter ( $T_H$ ) and receiver ( $T_L$ ). The radiative heat transfer rate,  $q_{\text{rad}}$ , is obtained by excluding the conduction from the total heat transfer rate measured by the heat flux meter with the assumption that all posts have the same height as the gap spacing. The radiative heat transfer coefficient is calculated from

$$h_{\text{rad}} = \frac{q_{\text{rad}}/A}{\Delta T}, \quad (1)$$

where the area  $A = 1 \text{ cm}^2$ , by neglecting the posts, and  $\Delta T = T_H - T_L$ .

Figure 2 displays  $q_{\text{rad}}$  for three different gap spacings versus  $\Delta T$ . The isolated solid symbols represent the measured results with uncertainty bounds indicated by the error bars.



The dashed lines are from the calculation with the shaded region indicating the uncertainty bounds. Fluctuational electrodynamics was used to calculate the near-field radiative heat transfer as discussed in the [supplementary material](#). The large enhancement in nanoscale thermal radiation is attributed to the excitation of coupled surface plasmon polaritons.<sup>1,2</sup> The uncertainty of the theoretical calculation is mainly due to the determination of the gap spacing. It can be seen that good agreement exists between the measurement and calculation: the differences are 5%, 17%, and 37% for gap spacing ( $d$ ) of 762 nm, 350 nm, and 200 nm, respectively. These are all within the combined uncertainties of the experiment and calculation. As  $d$  gets smaller, not only does  $q_{\text{rad}}$  become larger but also  $h_{\text{rad}}$  increases as evidenced by the increased slope. For a given gap spacing, the curve is not linear since measured  $h_{\text{rad}}$  increases slightly as the temperature increases. Different  $\Delta T$  is created by controlling the power of DC power supply. However, due to radiation from the top of the heater and conduction through the spring, not all the heating power flows down across the sample. For example, with a 265 mW power provided by the DC power supply, about 191 mW (134 mW due to radiation and 57 mW due to conduction) pass through the 200 nm sample, creating a  $\Delta T = 16.5^\circ\text{C}$ . The value  $q_{\text{rad}} = 134$  mW is considered the highest radiation heat transfer rate through submicron gap spacings measured to date.

Figure 3 illustrates the experimental results for  $h_{\text{rad}}$  for 14 measurements at different gap spacings. The measured data are presented as filled symbols with error bars, while the calculated values at the same temperature and gap spacings are shown as open circles. The 14 measurements were conducted using seven different samples. Some of the samples were measured under different applied forces since the gap spacing is sensitive to the applied force. Each shape of the solid symbols represents a different sample under

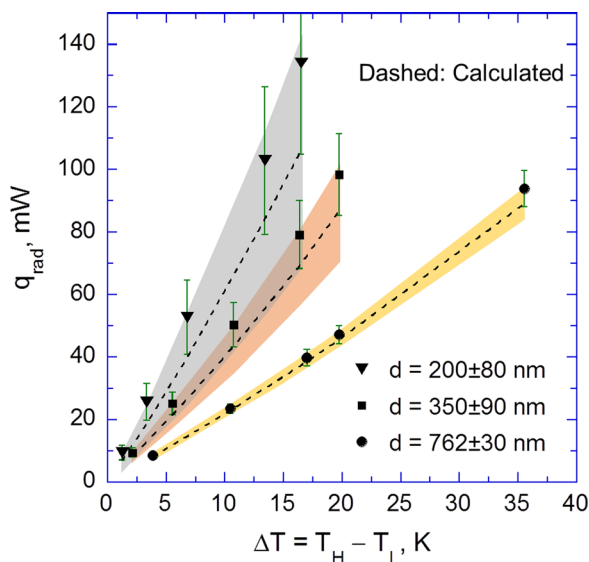


FIG. 2. Radiative heat transfer rate ( $q_{\text{rad}}$ ) for three different gap spacings as a function of the temperature difference. The filled symbols are the measured results with error bars. The dashed line represents the calculated  $q_{\text{rad}}$  based on the measured temperatures and gap spacing using fluctuational electrodynamics. The shaded regions show the uncertainty bounds of the calculated  $q_{\text{rad}}$ .

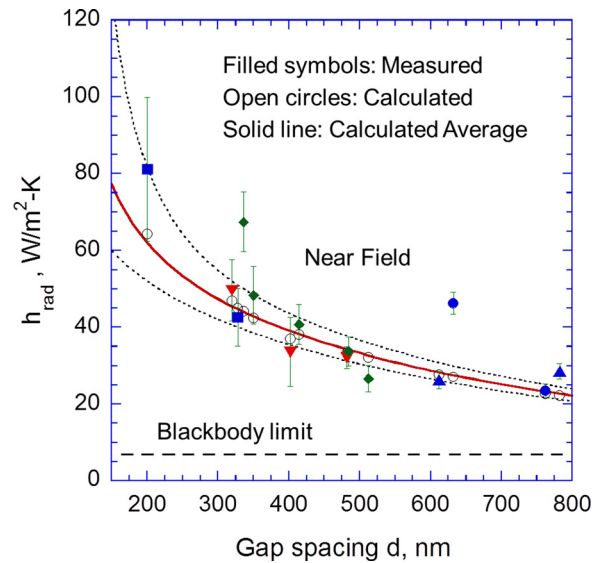


FIG. 3. Radiative heat transfer coefficient ( $h_{\text{rad}}$ ) for 14 measurements at different gap spacings with  $\Delta T$  ranging from 15.2 K to 19.2 K (except for the one at 402 nm spacing for which  $\Delta T = 9.8$  K). The filled symbols represent the measured results with error bars. Each shape denotes a specified sample under certain applied forces. The open circle is the calculated  $h_{\text{rad}}$  for each sample at the measured  $T_H$  and  $T_L$ . The solid red line is the  $h_{\text{rad,avg}}$  calculated from the average  $T_H$  (318.5 K) and  $T_L$  (302.3 K). The dotted lines are the uncertainty bounds of  $h_{\text{rad,avg}}$ . The dashed horizontal line is for two blackbodies at the average  $T_H$  and  $T_L$ .

specified applied forces. For example, the sample represented by the green diamond symbols is measured under different forces ranging from 0 mN to 200 mN to control the gap spacing from about 512 nm to 336 nm. The applied force and the sample used for each measurement are given in Table S1 (see [supplementary material](#)). The solid (red) line represents the calculated results using the average  $T_H$  and  $T_L$  (i.e., 318.5 K and 302.3 K, respectively) of all measurements and plotted as a function of gap spacing. The two dotted lines represent the calculation uncertainty bounds. The horizontal dashed line is the blackbody limit using the average  $T_H$  and  $T_L$ . A reasonable agreement between the experiment and calculation can be seen from Fig. 3. Note that  $h_{\text{rad}}$  increases as  $d$  decreases, reaching a value of  $81.2 \text{ W/m}^2\text{-K}$  that is about 11 times that of the blackbody limit at the same emitter and receiver temperatures. This value is nearly twice as high as those reported by Ito *et al.*<sup>24</sup> between fused quartz at their smallest gap spacing of 500 nm. The measured results at distances of 336 nm and 632 nm are much higher than the predictions; possible reasons for the disagreement will be discussed later.

While the  $\text{SiO}_2$  posts maintain the gap between the two Si pieces, the gap spacing is not necessarily equal to the height of the posts. In the experiment, the gap spacing can be higher than the post height by tens to a few hundreds of nanometers. Since the height of the posts are nearly uniform across the sample and their top surfaces are flat within about 30 nm based on measurements, possible reasons for the discrepancy are the residual bow or warp, unevenness of the post heights due to etching, and particles on the order of tens of nanometers. This effect also makes the gap spacing sensitive to external forces applied on the sample similarly as with a spring, offering a possible way to further control the

gap spacing through nearly elastic deformation. Therefore, in the experiment, we used a Fourier-transform infrared spectrometer (FTIR) to measure the reflectance of each sample to quantify the gap spacing prior to the heat transfer measurement. In some more recent measurements, different forces were applied for both the FTIR measurement and the heat transfer measurement, allowing the gap spacing to be adjusted.

As mentioned before, the sample contains two doped-Si slabs, about  $500\text{ }\mu\text{m}$  thickness, sandwiching a thin layer of vacuum or air. The spectral reflectance depends on the thickness of the middle layer due to interference effects, and thus the reflectance spectrum can be used to determine the gap spacing. The reflectance is insensitive to the thickness of the Si slabs since the FTIR resolution is not high enough to distinguish the interference fringes in the Si slab, which can be treated as incoherent.<sup>5</sup> This technique, however, requires the Si slab to be transparent at least in a certain frequency range for the infrared radiation to penetrate through and generate a distinguishable interference pattern. Meanwhile, the material is required to be opaque in the mid- and far-infrared range to have a considerable radiative heat flux. Calculations suggest that, for  $500\text{-}\mu\text{m}$ -thick Si wafers, a doping concentration from  $1 \times 10^{18}$  to  $3 \times 10^{18}\text{ cm}^{-3}$  can still be transparent at wavenumbers from  $2000\text{ cm}^{-1}$  to  $10000\text{ cm}^{-1}$  for FTIR measurements of the gap spacing, while at the same time can have sufficient free-carrier absorption at longer wavelengths for near-field radiative transfer enhancement.<sup>27,28</sup> Si wafers doped with antimony atoms of  $2 \times 10^{18}\text{ cm}^{-3}$  concentration were purchased from a commercial vendor. Their optical constants are extracted from the measured reflectance and transmittance of the wafer as well as extended to the mid- and far-infrared using a Drude model (see [supplementary material](#)). The doped-Si pieces can be treated as semi-infinite when considering the near-field radiative heat transfer, so that the backside oxide films and other materials at the contact have negligible effects on the radiative heat transfer. However, the oxide film does affect the measured FTIR spectrum as discussed next.

A fixture was manufactured and mounted on the reflectance accessory of the FTIR in order to apply different forces on the sample during the reflectance measurement in a similar manner as shown in Fig. 1(a) for heat transfer measurements. Considering the yield stresses of the  $\text{SiO}_2$  and Si, the applied force on the sample is limited to 200 mN. The gap distance is determined using a least-squares method by comparing the measured reflectance spectrum with the theoretical curves at different gap spacings. Figure 4 shows the measured and calculated reflectance spectra for three different gap spacings. The spectrum for the sample with 200 nm spacing is different since the patterned and the unpatterned piece have a silicon dioxide film of 595 nm and 785 nm, respectively, on the back sides. The gap spacing is determined such that the predicted spectrum at this gap spacing yields the smallest standard error of estimate compared to the measurement as discussed in the [supplementary material](#). After the gap spacing is fully characterized, the sample is mounted in the experimental setup to measure the thermal conductance with a force applied to achieve a desired gap spacing. While good agreement between the measurement and calculation is obtained for most data points shown in Fig. 3, it

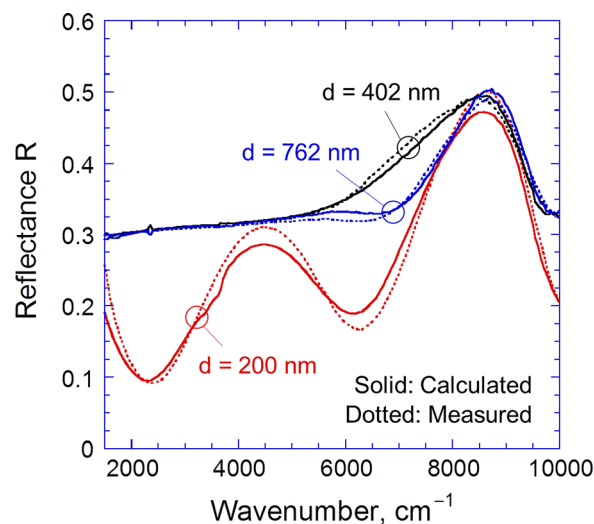


FIG. 4. Reflectance spectra for three samples with different gap spacings. The sample with a spacing of 200 nm has an oxide film of 595 nm and 785 nm on the back sides of the patterned and the unpatterned pieces, respectively.

should be noted that for the sample shown with diamond symbols, the reflectance spectra for  $260\text{ nm} < d < 340\text{ nm}$  are almost indistinguishable, which may explain the deviation of the measured result at 336 nm spacing. A smaller gap spacing than the prescribed value would increase the calculated  $h_{\text{rad}}$  and decrease the measured  $h_{\text{rad}}$ , making the agreement between them possible. This can be a limitation of using doped-Si in the current experiment, but may be alleviated when other materials are used. Note that the force needs to be applied with great care since an uneven distribution of forces can cause the sample to deform nonuniformly and create local bow that makes the gap spacing smaller than that determined by FTIR. This can cause a larger measured  $h_{\text{rad}}$  than the calculated value and could be the reason for the deviation of measurement at 632 nm spacing. Because the sample is contaminated by the grease after the thermal conductance measurement, they cannot be remeasured on the FTIR. The result for the 632 nm spacing is shown to stress the importance of handling the sample in the experiments.

The experimental results presented here demonstrate that the near-field effect can be probed with a heat transfer area at the square-centimeter scale and gap spacings down to about 200 nm. The high heat transfer rate achieved from this study may facilitate practical applications in energy conversion and thermal management devices based on near-field thermal radiation. With the development of this technique and future improvements, it is expected that accurate measurements can be made possible between various materials and nanostructures with even larger heat transfer areas that can potentially yield even stronger near-field heat transfer. Experiments of this nature and insights from such studies may signify breakthroughs in applications of near-field thermophotovoltaics, radiative cooling and refrigeration, and thermal rectifiers or transistors.

See [supplementary material](#) for details of sample fabrication, dielectric function, gap spacing determination, uncertainty analysis, and theoretical calculations.

This work was primarily supported by the U.S. Department of Energy, Office of Science, Basic Energy Science (DE-FG02-06ER46343). B.Z. and Z.M.Z. were also supported by the National Science Foundation (CBET-1235975; CBET-1603761). The facilities at Georgia Tech's Institute for Electronics and Nanotechnology (IEN) were used for the sample fabrication and some characterizations.

- <sup>1</sup>S. Basu, Y.-B. Chen, and Z. M. Zhang, *Int. J. Energy Res.* **31**, 689 (2007).
- <sup>2</sup>C. J. Fu and Z. M. Zhang, *Int. J. Heat Mass Transfer* **49**, 1703 (2006).
- <sup>3</sup>S. Shen, A. Narayanaswamy, and G. Chen, *Nano Lett.* **9**, 2909 (2009).
- <sup>4</sup>E. Rousseau, A. Siria, G. Jourdan, S. Volz, F. Comin, J. Chevrier, and J.-J. Greffet, *Nat. Photonics* **3**, 514 (2009).
- <sup>5</sup>Z. M. Zhang, *Nano/Microscale Heat Transfer* (McGraw-Hill, New York, 2007).
- <sup>6</sup>X. L. Liu, L. P. Wang, and Z. M. Zhang, *Nanoscale Microscale Thermophys. Eng.* **19**, 98 (2015).
- <sup>7</sup>R. S. DiMatteo, P. Greiff, S. L. Finberg, K. A. Young-Waithe, H. K. H. Choy, M. M. Masaki, and C. G. Fonstad, *Appl. Phys. Lett.* **79**, 1894 (2001).
- <sup>8</sup>C. R. Otey, W. T. Lau, and S. Fan, *Phys. Rev. Lett.* **104**, 154301 (2010).
- <sup>9</sup>L. P. Wang and Z. M. Zhang, *Nanoscale Microscale Thermophys. Eng.* **17**, 337 (2013).
- <sup>10</sup>P. Ben-Abdallah and S.-A. Biehls, *Phys. Rev. Lett.* **112**, 044301 (2014).
- <sup>11</sup>K. Chen, P. Santhanam, S. Sandhu, L. Zhu, and S. Fan, *Phys. Rev. B* **91**, 134301 (2015).
- <sup>12</sup>X. L. Liu and Z. M. Zhang, *Nano Energy* **26**, 353 (2016).
- <sup>13</sup>A. Kittel, W. Müller-Hirsch, J. Parisi, S.-A. Biehls, D. Reddig, and M. Holthaus, *Phys. Rev. Lett.* **95**, 224301 (2005).
- <sup>14</sup>S. Shen, A. Mavrokefalos, P. Sambegoro, and G. Chen, *Appl. Phys. Lett.* **100**, 233114 (2012).
- <sup>15</sup>J. Shi, P. Li, B. Liu, and S. Shen, *Appl. Phys. Lett.* **102**, 183114 (2013).
- <sup>16</sup>K. Kim, B. Song, V. Fernández-Hurtado, W. Lee, W. Jeong, L. Cui, D. Thompson, J. Feist, M. T. H. Reid, F. J. García-Vidal, J. C. Cuevas, E. Meyhofer, and P. Reddy, *Nature* **528**, 387 (2015).
- <sup>17</sup>B. Song, Y. Ganjeh, S. Sadat, D. Thompson, A. Fiorino, V. Fernández-Hurtado, J. Feist, F. J. Garcia-Vidal, J. C. Cuevas, P. Reddy, and E. Meyhofer, *Nat. Nanotechnol.* **10**, 253 (2015).
- <sup>18</sup>L. Hu, A. Narayanaswamy, X. Chen, and G. Chen, *Appl. Phys. Lett.* **92**, 133106 (2008).
- <sup>19</sup>R. S. Ottens, V. Quetschke, S. Wise, A. A. Alemi, R. Lundock, G. Mueller, D. H. Reitze, D. B. Tanner, and B. F. Whiting, *Phys. Rev. Lett.* **107**, 014301 (2011).
- <sup>20</sup>T. Kralik, P. Hanzelka, M. Zobac, V. Musilova, T. Fort, and M. Horak, *Phys. Rev. Lett.* **109**, 224302 (2012).
- <sup>21</sup>R. St-Gelais, B. Guha, L. Zhu, S. Fan, and M. Lipson, *Nano Lett.* **14**, 6971 (2014).
- <sup>22</sup>T. Ijoro and N. Yamada, *Appl. Phys. Lett.* **106**, 023103 (2015).
- <sup>23</sup>M. Lim, S. S. Lee, and B. J. Lee, *Phys. Rev. B* **91**, 195136 (2015).
- <sup>24</sup>K. Ito, A. Miura, H. Iizuka, and H. Toshiyoshi, *Appl. Phys. Lett.* **106**, 083504 (2015).
- <sup>25</sup>R. St-Gelais, L. Zhu, S. Fan, and M. Lipson, *Nat. Nanotechnol.* **11**, 515 (2016).
- <sup>26</sup>B. Song, D. Thompson, A. Fiorino, Y. Ganjeh, P. Reddy, and E. Meyhofer, *Nat. Nanotechnol.* **11**, 509 (2016).
- <sup>27</sup>S. Basu, B. J. Lee, and Z. M. Zhang, *J. Heat Transfer* **132**, 023301 (2010).
- <sup>28</sup>S. Basu, B. J. Lee, and Z. M. Zhang, *J. Heat Transfer* **132**, 023302 (2010).